Molecular Crystals and Liquid Crystals
Publication details, including instructions for authors and subscription information:
http://www.informaworld.com/smpp/title~content=t713644168

Infrared Spectra and Magnetic Properties of a Biaxial Nematic Bent-Core Liquid Crystal: Study of Conformations and Local Ordering in A131

Alberto Marini[a]; Ronald Y. Dong[b]
[a] Dipartimento di Chimica e Chimica Industriale, Universitá di Pisa, Italy [b] Department of Physics and Astronomy, University of British Columbia, Vancouver, BC, Canada

First published on: 13 July 2010

To cite this Article Marini, Alberto and Dong, Ronald Y.(2010) 'Infrared Spectra and Magnetic Properties of a Biaxial Nematic Bent-Core Liquid Crystal: Study of Conformations and Local Ordering in A131', Molecular Crystals and Liquid Crystals, 525: 1, 74 — 96
To link to this Article: DOI: 10.1080/15421401003796058
URL: http://dx.doi.org/10.1080/15421401003796058

Mol. Cryst. Liq. Cryst., Vol. 525: pp. 74–96, 2010

ISSN: 1542-1406 print/1563-5287 online
DOI: 10.1080/15421401003796058

Taylor & Francis
Taylor & Francis Group

Infrared Spectra and Magnetic Properties of a Biaxial Nematic Bent-Core Liquid Crystal: Study of Conformations and Local Ordering in A131

ALBERTO MARINI[1] AND RONALD Y. DONG[2]

[1]Dipartimento di Chimica e Chimica Industriale, Universitá di Pisa, Italy
[2]Department of Physics and Astronomy, University of British Columbia, Vancouver, BC, Canada

Density functional theory (DFT) has been employed in a detailed conformational study of a bent-core mesogen (A131), in order to shed light on its uniaxial-biaxial nematic phase transition, questioned recently in the literature. Two distinct computed structural groups, namely the Banana-shaped (BS) and the Hockey Stick-shaped (HSS) forms, were found to give different theoretical infrared spectra and magnetic susceptibility tensors, suitable to potentially distinguish between the two nematic phases. GIAO-DFT chemical shielding tensors (CSTs) of the aromatic carbons, found in agreement with those experimentally measured by the 2D-NMR SUPER technique, were used to provide new structural and local orientational order parameters of A131.

Keywords Banana shaped LC; biaxial nematics; chemical shift sensors; conformations; DFT calculations; infrared spectra; magnetic susceptibility

I. Introduction

The biaxial nematic phase has long been sought for in thermotropic Liquid Crystals (LC) since its prediction by Freiser in 1970, [1] and its experimental confirmation by Yu and Saupe in 1980 of a uniaxial to biaxial nematic phase transition in a lyotropic ternary system [2]. Various attempts to search for this phase in new LC materials composed of calamitic molecules with increasingly anisometric character have led to much disappointment [3]. However, bent-core LC have recently shown great promise in rendering biaxial nematic (N_b) phases [4–6]. These new V-shaped molecules can also form the traditional uniaxial (N_u) phase [7–10] and the so-called banana phases. The identification of phase biaxiality in nematogens is by no means trivial and still is a matter of debate. Deuterium Nuclear Magnetic Resonance (NMR) has been successfully used to quantify the phase biaxiality in N_b phase [2–4].

The uniaxial and biaxial nematic phases exhibited by bent-core molecules have been theoretically investigated using a number of techniques, including (i) a molecular field analysis for symmetric bent-core molecules interacting via a continuous

Address correspondence to Alberto Marini, Dipartimento di Chimica e Chimica Industriale, Universitá di Pisa, Italy. E-mail: am@ns.dcci.unipi.it

potential [3], (ii) a bifurcation analysis of symmetric bent spherocylinders with purely repulsive interactions [11] and, more recently, (iii) a simulation study based on a bent-core Lebwohl-Lasher model in which symmetric models and deviations from these were investigated [12]. For the symmetric models, all three of these studies agree that the Landau point, at which the isotropic liquid undergoes a transition directly into the biaxial nematic, is predicted to occur when the bend angle Θ is at the tetrahedral angle of 109° 28′. The bend angle is the angle subtended by the two lateral wings next to the central ring and is one of the most important structure parameters in V-shaped molecules. Even a slight asymmetry in the molecule can adjust the Θ angle from the ideal tetrahedral angle. Recently, there have been some works by Bates [13] on V-shaped molecules, where a generic model for rigid V-shaped molecules is extended to include a bending potential, which allows to investigate the relationship between the flexibility of a bent-core molecule and its ability to form a biaxial nematic phase. The simulation results indicate that, as the flexibility is increased, the biaxial nematic phase is typically forced to lower temperatures (T). On the contrary, the stability of the uniaxial nematic phase with respect to the isotropic phase is not significantly affected. In addition, conformational flexibility that changes the mix of rodlike and disklike structures can have an effect on the $T - \Theta$ phase diagram.

In 2005, several other bent-core LC were found, based mainly on X-rays studies, to exhibit the N_b phase [14]. The $N_u - N_b$ phase transition is reported at 422 K in a particular asymmetric V-shaped molecule 2-methyl-3-[4-(4-octyl-benzoyloxy)-benzylidene]-amino-benzoic acid 4-(4-dodecyl-phenylazo)-phenyl ester (A131), whose molecular structure is shown in Figure 1(a). The same sample was later studied by ^{13}C solid-state NMR (ss-NMR) techniques [15] and the preliminary results are consistent with the existence of the $N_u - N_b$ transition upon cooling down from the clearing point. The Θ angle in the bent-core was also estimated to be 133° in this report.

In this study, detailed Density Functional Theory (DFT) calculations on the bent-core A131 were carrried out to provide the conformation energy landscapes, where two distinct computed structural groups, namely the Banana-shaped (BS) and the Hockey Stick-shaped (HSS) forms, were found. From a structural point of view, the arms of the investigated bent-core molecule are not identical, and therefore the interactions between similar and different arms will be different. Moreover, the present DFT study reveals that A131 molecule is quite flexible in its short lateral arm and can adopt more than one conformation, which could change the transition temperature(s) between the isotropic – uniaxial nematic – biaxial nematic phases.

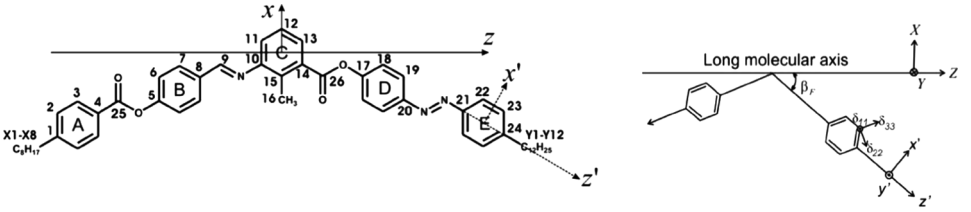

(a) (b)

Figure 1. (a) Molecular structure of A131 with carbon site labels, (b) Schematic of a CSA (δ_{11}, δ_{22}, δ_{33}) PAS frame, a fragment (x', y', z'), and a molecular frame (x, y, z) fixed on the molecule.

Furthermore, our NMR data point to different conformations becoming dominant in different phases.

The chemical shielding tensors of all the carbon atoms in the aromatic core of A131 had been calculated for the four optimized conformers [16]. This is partly prompted by a recent report which has questioned the existence of the $N_u - N_b$ transition in A131 [17] using electro-optic techniques, and has casted doubt on the X-rays finding and the ^{13}C chemical shift data in the bulk A131 sample. In this regard, a careful analysis of the ^{13}C data is warranted within the context of DFT approach. The combined DFT and ^{13}C chemical shift analyses are discussed in conjunction with DFT calculated Infrared (IR) spectra and Magnetic Susceptibilities Tensors (MSTs). One of the aims is to give additional insights on the local order parameters, in particular near the $N_u - N_b$ phase transition, and on the possible transformation among molecular core conformers in the nematic phase(s) of A131. The latter may well be detected by the shifts in frequencies seen in the calculated Infrared spectra, which could provide incentives for future experiments.

II. Theory

A brief description of the pertinent DFT methods and NMR chemical shifts in mesophases is given here, as details can be found in the literature. Direct implementation of the Gauge Invariant Atomic Orbitals (GIAO) and the Continuous Set of Gauge Transformations (CSGT) methods [18] for calculating nuclear magnetic shielding tensors at both the levels of Hartree-Fock (HF) and DFT have been presented and discussed in Ref. [19]. The GIAO (in Gaussian 03) [20] was first introduced by Ditchfield within the coupled HF scheme [21]. The components σ_{ij} of nuclear shielding tensor (CST) of a carbon nucleus are related to corresponding ones δ_{ij} of the measured carbon chemical shift anisotropy (CSA) tensor according to the following relation:

$$\sigma_{ij} = K_{ij}\sigma_{ref} - \delta_{ij} \tag{1}$$

where the offset value, σ_{ref}, corresponds to the isotropic shielding of a reference compound, and K_{ij} is the Kronecker delta. The isotropic shielding of the reference compound is either estimated from a gas-phase measurement or assumed from DFT calculations (see below). In order to compare the calculated CSA data with those reported in literature, we have decided to denote the principal elements of the symmetric part of the chemical shift tensor by $\delta_{33} \geq \delta_{22} \geq \delta_{11}$ (this convention states that δ_{33} corresponds to the direction of the least shielded, σ_{33}, with the highest frequency or highest shift).

The local order parameters S' and D' can be obtained in a mesophase from the observed ^{13}C shifts $\langle\delta\rangle$ in a ring fragment of the studied molecule according to [22]

$$\langle\delta\rangle = \delta_{iso} + \frac{2}{3}S'[P_2(\cos\beta)(\delta_{33} - \delta_{22}) + \frac{1}{2}(\delta_{22} - \delta_{11})] + \frac{1}{3}D'[\delta_{11} - \delta_{22}\cos^2\beta - \delta_{33}\sin^2\beta] \tag{2}$$

where δ_{ii} are the principal components of the carbon CSA tensor in its Principal Axis System (PAS), β is the angle between the orientation of δ_{33} with the z' axis of the

fragment, S' represents the local nematic order S of the para axis, and D' represents the local (fragmental) biaxial ordering ($S_{xx} - S_{yy}$) w.r.t. the (x', y', z') (see Fig. 1(b)) frame attached on the fragment. These local order parameters (S' and D') for the lateral phenyl rings of A131 can be deduced by fitting the observed ^{13}C chemical shifts from each fragment given by the above equation. In the following, the superscripts on S' and D' will be omitted for simplicity, with the understanding that they refer to local ordering of each aromatic fragment. Phase biaxiality (quite different from D) is, however, undetectable [22] for an aligned sample of $\Delta\chi > 0$ as in the case of A131.

The central ring of A131 needs some attention as it cannot flip or rotate like the lateral phenyl rings, thereby possessing a reduced (C_s) symmetry. As a result, the Saupe order matrix in the chosen molecular (x, y, z) frame (see Fig. 1(a)) is not diagonal. In other words, there are three nonzero order parameters S_{zz}, $S_{xx} - S_{yy}$ and S_{xz}. The last order parameter is, however, usually vanishingly small. Even so, this local order tensor (in the (x, y, z) frame) can be fully determined from the five ^{13}C $\langle\delta\rangle$'s obtained for the central ring of A131 using the following equation:

$$\langle\delta\rangle = \delta_{iso} + \frac{2}{3}\left[\Delta\delta S_{zz} + \frac{1}{2}(\delta_{xx} - \delta_{yy})(S_{xx} - S_{yy}) + 2\delta_{xz}S_{xz}\right] \tag{3}$$

where S_{xy} and S_{yz} are zero for symmetry reasons and $\Delta\delta$, the anisotropy of δ with respect to the chosen z axis, is given by

$$\Delta\delta = \delta_{zz} - \frac{1}{2}[\delta_{xx} + \delta_{yy}] \tag{4}$$

and the δ tensor of each carbon can be related to its PAS values by using

$$\delta_{ij} = \sum_{\eta} \cos\theta_{\eta i} \cos\theta_{\eta j}\delta_{\eta\eta} \tag{5}$$

where $\theta_{\eta i}$ is the angle between the PAS η axis and the fragment i axis. To determine either molecular or local order parameters from the ^{13}C chemical shifts in LC requires the precise knowledge of CSA tenors and their PAS's orientations, both of which can be obtained by DFT calculations.

III. Experimental and Computational Details

The A131 sample was that used in Ref. [14]. Its transition temperatures (K) are: I (449.5) N_u (422) N_b (391.5) SmC (377.3) SmX (366.4) SmY (355.8) Cr. All the information concerning the ^{13}C NMR solution and solid state measurements have been detailed and discussed elsewhere [15]. In this work, all the DFT calculations have been performed using Gaussian 03 package [20], where all the molecular models were built by means of GaussView 3.0 program. To shed further light on the experimental NMR work of A131 mesogen [15], we have carried out the following computational strategy. DFT calculations have been performed to obtain the most populated conformational states within its five-ring molecular core, at in vacuo DFT level of theory employing the B3LYP [23] functional in combination with the polarized 6–31 + G(d) basis set throughout the different geometry optimizations. Geometries obtained in this way are at least as good, and in several cases

(such as phenyl-benzoate) better than those obtained at the Möller Plesset theory MP2/6-31 + G(d) level [24]. The calculated Potential Energy Surface (PES) has revealed four prevalent conformers for which the IR frequencies were calculated at B3LYP/6-311 + G(d,p) level of theory (here a larger basis set has been used). In particular, the Gaussian output files were processed by an utility function in GaussView program that extracted fundamental frequencies and corresponding IR intensities to simulate the calculated IR spectra as a sum of Lorentzian functions. In this case, the simulated IR bands had $10\,cm^{-1}$ band widths (FWHH). DFT approach (with a suitable choice of both functional and basis sets), which has a computational cost of the same order as Hartree Fock (HF), considerably less than traditional correlation techniques, often gives quality calculations comparable to or even better than those of MP2 [25]. Moreover, the DFT method is generally preferred in view of the lesser sensitivity on the basis set and of its computational convenience in particular. The modified Perdew-Wang [26] exchange-correlation functional, called MPW1PW91 [27] is particularly accurate in predicting magnetic properties, and is therefore used here for both the calculations of molecular magnetic susceptibility and the chemical shielding tensors. Moreover, for their numerous advantages [28], we have decided to adopt the CSGT (Continuous Set of Gauge Transformations) and the GIAO (Gauge Including Atomic Orbitals) [21] for calculating magnetic susceptibilities and chemical shielding tensors, respectively. Finally, a suitable choice for referencing is required to relate the carbon chemical shielding values (σ scale) and NMR chemical shifts (δ shift scale), which are referenced to some standard such as TMS. Now the chemical shielding σ^{ref} of the reference can be computed. In particular, the CSA tensors can be obtained by referencing the absolute CSTs obtained by DFT to the absolute shielding of TMS (185.97 ppm), which is calculated at the same level of theory as for the various models of A131. It is noticed that the value of δ_{iso} for TMS obtained by GIAO-DFT calculations is very close to the experimental value for TMS (185.4 ppm) obtained after correction of vibrational averaging, bulk susceptibility, temperature, and relating to a secondary standard [29]. This result confirms the appropriateness of the basis set and functional used in our GIAO-DFT calculations.

A. Conformational Analysis

Preliminary tests on a full A131 molecule have shown that the torsional energies are almost independent of the length of the aliphatic chains. Thus, a 5-rings (**5R**) molecular model, namely the 2-methyl-3-[4-(4-methyl-benzoyloxy)-benzylidene]-amino-benzoic acid 4-(4-methyl-phenylazo)-phenyl ester (**ABCDE** model), shown in Figure 2(a) has been adopted. In this way it was possible to investigate A131 molecule with an accurate description of its electronic structure, offered by a high level Quantum Mechanical (QM) approach. All the details regarding the conformational analysis have been reported in Ref. [30]; here only a brief summary of the main results is given.

In order to lower the computational cost, PES is surveyed initially using 3-rings (**3R** model) fragments (i.e., **ABC, BCD, CDE**). For computational and molecular complexity reasons, it has been decided to select the dihedrals which can reasonably influence the conformations of A131 molecule. Several conformational studies on V-shaped molecules have, therefore, been considered in order to choose the proper

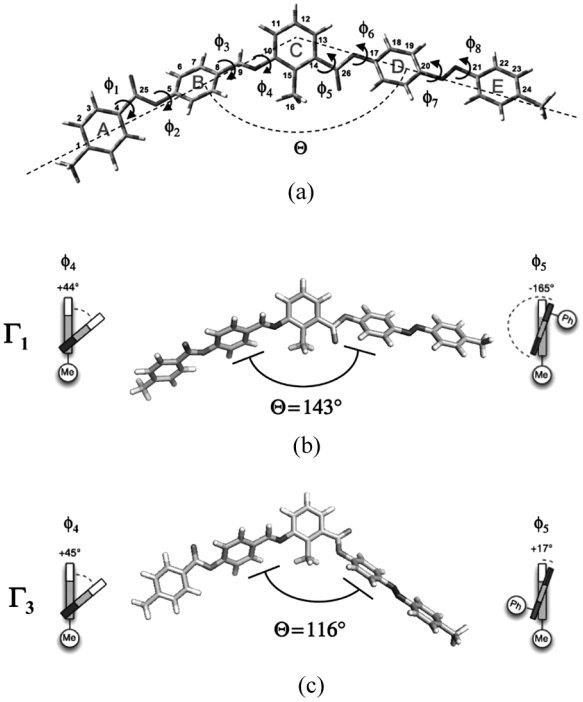

Figure 2. (a) Molecular structure of a **ABCDE** 5-ring **5R** model of A131 mesogen together with the bend angle Θ and dihedral angles ϕ_i. (b) Graphs showing two of the four relevant conformations $\boldsymbol{\Gamma_1}$, $\boldsymbol{\Gamma_2}$, $\boldsymbol{\Gamma_3}$ and $\boldsymbol{\Gamma_4}$ of A131. Note that $\boldsymbol{\Gamma_1}$, and $\boldsymbol{\Gamma_4}$ show a BS configuration, while $\boldsymbol{\Gamma_2}$ and $\boldsymbol{\Gamma_3}$ give the HSS structure.

angles and to obtain reliable results, once given a reasonable thermal energy at the disposal of the mesogen [30]. Specifically, the dihedral angles the $C_{25}-O-C_5-C_6$ (ϕ_2) and $C_9-N-C_{10}-C_{11}$ (ϕ_4) were scanned in **ABC**, the $C_9-N-C_{10}-C_{11}$ (ϕ_4) and $C_{13}-C_{14}-C_{26}-O$ (ϕ_5) dihedrals for **BCD**, and the $C_{13}-C_{14}-C_{26}-O$ (ϕ_5) and $C_{19}-C_{20}-N-N$ (ϕ_7) dihedrals for **CDE**. Relevant information on torsional barriers and conformational states in each **3R** model were obtained. The PES(**BCD**) shows the highest rotational barriers found among the **3R** models investigated. Indeed the conformations of **BCD** model are important in determining the orientations of the lateral wings and the bend angle of the entire molecule, because the ϕ_4 and ϕ_5 dihedrals are expected to play a major role in determining the prevalent conformational states in the A131 molecule.

Four basins of attraction obtained in the PES(**BCD**) have been surveyed in the **ABCDE** (**5R**) model. Reliable conformers of the **5R** model have been built up in these basins of attraction (in the PES(**BCD**)) by exploiting all the information gained in the conformational study of the **3R** models. The four wide basins are characterized by quite low energy regions (less than 2.5 kcal/Mol), and separated by high energy barriers (from 6 to 12 kcal/Mol). The eight symmetry related conformers $\boldsymbol{\Gamma}_i$ (see Table 1) were subsequently optimized without constraints in geometry in order to obtain fully relaxed structures for the **5R** model, at the same level of theory used for the **3R** models.

Table 1. Structural parameters: dihedral and bend angles (in degrees), relative energies (in kcal/Mol) and populations (in %) for Γ_i conformers of the **ABCDE** 5-rings model

Conformation	ϕ_2 (°)	ϕ_4 (°)	ϕ_5 (°)	ϕ_7 (°)	ϑ (°)	ΔE (kcal/Mol)	P (%)
Γ_1	43	44	−165	0	143	0.000	28.5
Γ_2	42	45	−18	0	115	1.076	4.7
Γ_3	42	45	17	0	116	1.413	2.65
Γ_4	43	44	166	0	146	0.417	14.15
Γ_5	43	−44	−166	0	146	0.417	14.15
Γ_6	42	−45	−17	0	116	1.413	2.65
Γ_7	42	−45	18	0	115	1.076	4.7
Γ_8	43	−44	165	0	143	0.000	28.5

These fully relaxed and optimized geometries lead to structural parameters very similar to those found for the minimum-energy conformers of **BCD** model, confirming that (i) the last configurations of **5R** model are good for interpreting the conformational behaviors of the full molecule, and (ii) conformations of the **A** and **E** rings have only small influences on the main conformational states of the central core. The in vacuo energy and population for various dominant (symmetry related to ϕ_4 and ϕ_5) conformers are also summarized in Table 1. As far as the ϕ_2 and ϕ_7 dihedrals are concerned, for each $\Gamma_\mathbf{i}$ found there are at least 8 other (4 principal states for $\phi_2 \times 2$ principal states for ϕ_7) populated conformations, not reported here because of symmetry reasons. The structural parameters found for ϕ_2 and ϕ_7 in the $\Gamma_\mathbf{i}$ conformers are in agreement with those found for the most populated conformers in PES(**ABC**) and PES(**CDE**), in particular the values of $\phi_2 \approx 45°$ and $\phi_7 = 0°$ represent conformations of the lowest energy in these **3R** models. The final full-optimized conformers $\Gamma_\mathbf{1}$, $\Gamma_\mathbf{2}$, $\Gamma_\mathbf{3}$ and $\Gamma_\mathbf{4}$ have been adopted to calculate the CSTs at the GIAO-DFT level. It has to be noticed that in vacuo, $\Gamma_\mathbf{1}$ and $\Gamma_\mathbf{4}$ (as well as the symmetry related $\Gamma_\mathbf{5}$ and $\Gamma_\mathbf{8}$) conformers are more predominant compared to the others. The molecular structures of $\Gamma_\mathbf{1}$ and $\Gamma_\mathbf{3}$ conformers, shown in Figure 2(b), show very different shapes with bend angle of 143° and 116°, respectively. It should be realized that the computed in vacuo conformational populations (e.g., for $\Gamma_\mathbf{4}$) may be drastically altered in the condensed phases due to intermolecular interactions.

The Θ angle has been reported for A131 [17] as 134° using MOPAC (Molecular Orbital PACkage), a quantum chemistry program based on Dewar and Thiel's NDDO (Neglect of Diatomic Differential Overlap) approximation. Relatively large errors were noted [31] in primarily organic molecules composed of H, C, N, O and halogen atoms when using AM1 and PM3 to evaluate bond lengths, dihedral or valence angles. Moreover, the semiempirical rotational barriers are consistently underestimated when compared with experiment. This may be attributed to a possible inadequacy of the MNDO (Modified Neglect of Diatomic Overlap)/AM1/PM3 empirical nuclear repulsion functions for describing transition state structures. In particular, corrected molecular structures depend on the proper location of potential wells in the PES, and they are intimately related to the energetics of conformational analyses, [32] as found in the present study by DFT methods. All this considered, the

reason for the difference in the bend angle reported in Ref [17]. can likely be ascribed to both the semiempirical and the single-conformer nature of the AM1 calculations.

B. Infrared Spectra Calculations

The in vacuo DFT calculated IR spectra of the four Γ_i conformers of A131 are shown in Figure 3, where the IR spectra of Γ_1 and of Γ_2 (shown in positive intensities) are compared with those of Γ_4 and of Γ_3 (shown in negative intensities merely for convenience), respectively. From this figure it is evident that the frequencies and intensities of the calculated IR spectra depend on the shape assumed by A131 molecule; thus IR spectra of BS are different from those obtained for HSS conformers, as clearly shown in Figure 4 for a direct comparison between that of Γ_1 and Γ_2). A complete vibrational assignment of the calculated (and opportunely scaled according to Ref. [33]) IR harmonic frequencies has been performed as reported in Tables 2 and 3 for the Fingerprint ($500 \div 1200\,cm^{-1}$) and the Functional Group ($1200 \div 3200\,cm^{-1}$) regions, respectively. In particular, the spectral regions between $1400 \div 1800\,cm^{-1}$ and between $2800 \div 3200\,cm^{-1}$ seem able to reflect the main conformational changes from BS to HSS conformation in A131.

The frequencies most affected by this conformational change are those related to the vibration of carbonyl, between both C-D rings [ν C=O (C∩D)] and A-B [ν C=O

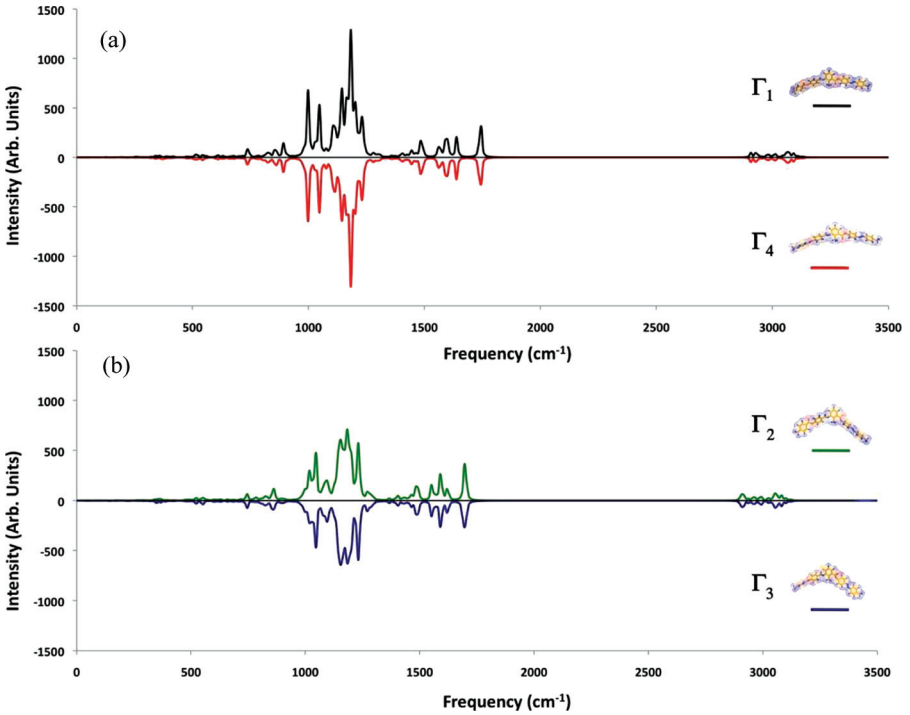

Figure 3. Comparison between in vacuo IR spectra calculated at B3LYP/6–311 + G(d) level of theory for the BS (a) and the HSS (b) conformers. The intensity on the y-axis is in arbitrary units: in order to facilitate the comparison, positive and negative intensity values have been adopted for Γ_1/Γ_4 and to Γ_2/Γ_3, respectively.

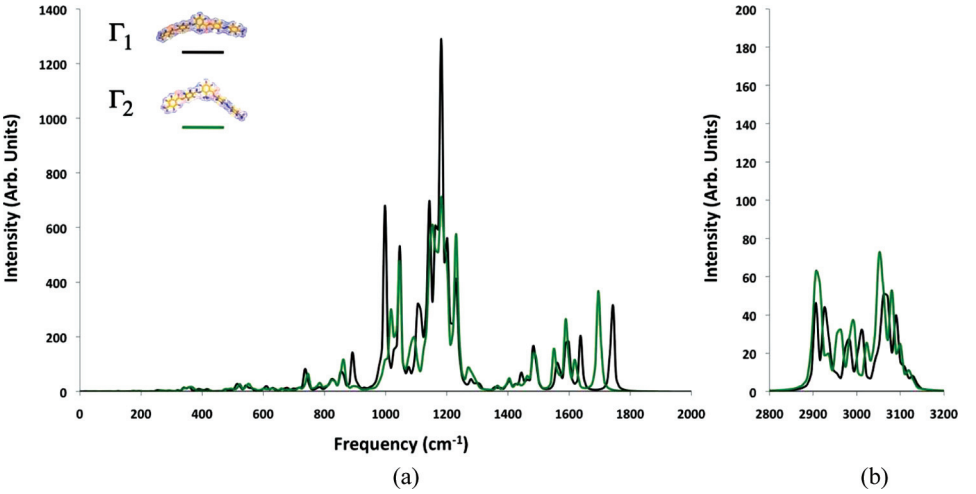

Figure 4. Comparison between in vacuo Infrared spectra, calculated at B3LYP/6–311 + G(d) level of theory, of $\boldsymbol{\Gamma_1}$ and $\boldsymbol{\Gamma_2}$ conformations in two different spectral ranges: (a) $0 \div 2000\,cm^{-1}$ and (b) $2800 \div 3200\,cm^{-1}$.

(A∩B)] rings, with a variation of about $40\,cm^{-1}$; similar variations are obtained for the symmetric stretching of the imminic unit [ν_s HC=N– (B∩C)]. Moreover, smaller variations of about $10\,cm^{-1}$ are shown by the symmetric stretching involving the diazo group [ν_s C–N=N–C (D∩E)] and by both the symmetric and the asymmetric stretching of CH_2 and CH_3. All the other frequencies calculated at DFT level of theory seem to be only slightly affected, more so in the peak intensities than in their frequencies.

On the contrary, the aim of the vibrational study concerning the low energy region is to elucidate the skeletal normal modes. In particular, the stretching or bond angle distortion has a higher participation in the description of the normal mode. In this IR region, eventual differences between theoretical and experimental spectra could be used to elucidate the presence of possible intermolecular effects in both the crystalline and LC phases, via the overall molecular vibration distortions due to the symmetry of the LC phase.

Moreover, to study the orientational order from IR spectra, several bands could be of potential interest for the analysis of alignment of A131 [34]: (i) the phenyl CC stretching vibrations in the range of 1500–1600 cm^{-1}, (ii) the phenyl CH out of-plane vibrations close to 700–900 cm^{-1}, (iii) the symmetric stretching of the imminic unit in the range of 1600–1650 cm^{-1} and (iv) the stretchings of the different carbonyl units in the range of 1700–1750 cm^{-1}. Transition dipole moments for the CC ($\sim$1600 cm^{-1}) stretching vibrations are oriented parallel to the core plane, while for the CH out-of-plane vibration ($\sim$800 cm^{-1}) the transition dipole moment is oriented perpendicular to the core plane. Thus, the bands of the phenyl CC stretchings and the phenyl CH out of-plane vibrations are the most sensitive indicators of ordering of the aromatic rings as their intensities are directly correlated with the core-core order.

Finally, we suggest that the calculated IR spectra of the two main conformational states of A131, BS and HSS, could shed further lights on the possible shapes

Table 2. Fingerprint region ($500 \div 1200\,cm^{-1}$) of the DFT calculated IR frequencies [cm^{-1}] (opportunely scaled by a factor 0.9688, according to Ref. [33]) and intensities in arbitrary units [arb. units] corresponding to the theoretically assigned normal modes $\tilde{\nu}$, labelled with the following abbreviation: ν, stretching; δ, bending; ω, wagging; γ, out-of-plane bending; ρ, rocking; τ, torsion. A,B,C,D,E refer to the aromatic rings labelling. Z (X∩Y) identifies the functional group Z between X and Y rings. The labels *w*, *m*, *s* refer to weak, medium and strong intensity values

Assignment	Freq. [cm^{-1}]	Intensity (Γ_1) [arb. units]	Intensity (Γ_4) [arb. units]	$\tilde{\nu}$ Intensity	Freq. [cm^{-1}]	Intensity (Γ_2) [arb. units]	Intensity (Γ_3) [arb. units]	$\tilde{\nu}$ Intensity
τ (DE)	503.8	16.1	16.1	w	513.5	12.2	12.2	w
	523.2	19.1	21.5	w	523.2	29.5	29.7	w
	542.5	27.5	27.5	w	552.2	36.8	35.7	w
τ (AB)	600.7	13.2	13.2	w	600.7	12.1	12.3	w
	610.4	20.5	20.5	w	610.4	7.9	7.7	w
τ (CD)	629.7	15.3	15.3	w	629.7	11.2	11.4	w
	658.8	13.6	13.7	w	658.8	10.0	9.8	w
	678.2	15.8	15.8	w	687.9	9.6	9.4	w
γ CH (A) + ρ CH_3 (A)	726.6	16.1	15.7	w	726.6	9.4	9.7	w
	736.3	82.8	72.6	w	736.3	27.6	27.8	w
	746.0	39.3	26.0	w	746.0	65.3	65.8	w
γ CH (A,E)	775.0	12.5	14.7	w	775.1	13.2	12.9	w
	784.7	16.5	18.6	w	784.7	31.9	30.4	w
	794.4	9.2	15.2	w	804.1	27.1	26.3	w

(*Continued*)

Table 2. Continued

Assignment	Freq. [cm^{-1}]	Intensity (Γ_1) [arb. units]	Intensity (Γ_4) [arb. units]	$\tilde{\nu}$ Intensity	Freq. [cm^{-1}]	Intensity (Γ_2) [arb. units]	Intensity (Γ_3) [arb. units]	$\tilde{\nu}$ Intensity
γ CH (B,C,D)	804.1	15.0	29.7	w	813.8	24.2	24.8	w
	813.8	27.7	29.7	w	823.5	42.0	42.3	w
	823.5	45.9	50.6	w	833.2	37.5	38.3	w
γ CH (C) + ρ CH_3	891.3	143.0	147.7	m-w	852.5	65.8	66.1	m-w
	988.2	165.0	178.0	m-w	862.2	117.3	118.2	m-w
ν_s COR + ω CC (C) + ν CCC	997.9	680.4	645.4	m	997.9	114.8	115.2	m-w
τ CH_3 (C) + ν_{as} COR	1007.6	123.4	158.0	m-w	1017.2	300.1	224.4	n
ν_s COR + ω CC (C) + ω CH (C,B)	1026.9	154.3	125.8	m-w	1046.3	477.1	467.7	m-s
ν_s COR + ω CH (B)	1036.6	171.7	145.3	m-w	1056.0	108.5	106.1	m-w
ν_s CN + ω CH (D,E)	1046.3	532.4	558.8	m	1123.8	151.2	146.2	m-w
ν_s CN + ω CH (A,B)	1104.4	319.2	292.6	m-w	1133.5	227.9	224.9	m-w
ω CH (A,B) + ω CC (A,B)	1114.1	299.9	345.9	m-w	1143.2	491.5	513.5	m-s
	1143.2	698.1	640.9	m-s	1152.9	610.3	642.2	s
	1162.6	607.8	581.2	m-s	1162.6	518.7	565.7	s
ω CH (D,E) + ω CC (D,E)	1172.2	594.2	581.7	m-s	1181.9	712.3	627.2	s
	1181.9	1290.2	1308.3	s	1191.6	541.8	559.3	s
	1191.6	480.0	535.2	m	1201.3	460.2	470.3	s

Table 3. Functional Group region ($1200 \div 3200\,cm^{-1}$) of the DFT calculated IR frequencies [cm^{-1}] (opportunely scaled by a factor of 0.9688, according to Ref. [33]) and intensities in arbitrary units [arb. units] corresponding to the theoretically assigned normal modes $\tilde{\nu}$, labelled with the following abbreviation: ν, stretching; δ, bending; ω, wagging; γ, out-of-plane bending; ρ, rocking; τ, torsion. A,B,C,D,E refer to the aromatic rings labelling; Z (X∩Y) identifies the functional group Z between X and Y rings. The labels *w*, *m*, *s* refer to weak, medium and strong intensity values

Assignment	Freq. [cm^{-1}]	Intensity (Γ_1) [arb. units]	Intensity (Γ_4) [arb. units]	$\tilde{\nu}$ Intensity	Freq. [cm^{-1}]	Intensity (Γ_2) [arb. units]	Intensity (Γ_3) [arb. units]	$\tilde{\nu}$ Intensity
ω CH (D,E) + ν_s CC + ν_s COR	1230.4	412.2	431.7	m	1230.4	576.7	594.3	s
δ_s CH_3 (C)	1414.4	21.5	25.5	w	1240.1	223.2	223.6	m-w
δ_{as} CH_3 (C)	1424.1	28.2	26.0	w	1404.8	48.6	49.9	w
δ_s CH_3 (A,E)	1443.5	69.5	68.5	w	1433.8	29.8	27.7	w
δ_{as} CH_3 (A,E)	1462.9	44.3	43.8	w	1462.9	57.8	63.9	w
δ_s + γ_s (D,E)	1482.3	166.3	166.3	m-w	1482.3	140.1	133.5	m-w
ω CC (DE,AB)	1492.0	106.0	108.9	w	1492.0	126.1	131.3	m-w
ν_{as} + ω CC=O (DE, AB)	1501.6	33.7	34.8	w	1501.6	39.7	40.9	w
ν_s C–C (C)	1559.8	103.8	104.1	w	1550.1	156.8	155.6	m-w
ν_s C–C (D) + ν_s C–C (E)	1569.5	81.3	80.1	w	1559.8	81.8	82.4	w
ν_{as} C–C (B) + ν_s HC=N	1588.8	174.9	175.1	m-w	1579.1	70.7	70.5	w
ν_s C–N=N–C (D∩E)	1598.5	182.3	185.1	m-w	1588.8	265.2	262.2	m-w
ν_s HC=N– (B∩C)	1637.3	204.4	222.6	m-w	1598.5	126.6	125.5	m-w

(*Continued*)

Table 3. Continued

Assignment	Freq. [cm^{-1}]	Intensity (Γ_1) [arb. units]	Intensity (Γ_4) [arb. units]	$\tilde{\nu}$ Intensity	Freq. [cm^{-1}]	Intensity (Γ_2) [arb. units]	Intensity (Γ_3) [arb. units]	$\tilde{\nu}$ Intensity
ν C=O (C∩D)	1734.2	151.4	183.5	m-w	1695.4	367.1	266.8	m-w
ν C=O (A∩B)	1743.8	315.2	271.0	m-w	1705.1	170.1	148.0	m-w
ν_s CH (HC=N)	2906.4	46.1	46.1	w	2906.4	62.5	61.6	w
ν_s CH_3 (E)	2925.8	43.8	45.3	w	2916.1	55.3	54.3	w
ν_s CH_3 (A)	2935.5	29.5	28.5	w	2954.8	30.0	30.4	w
ν_s CH_3 (C)	2945.2	12.0	10.2	w	2964.5	31.9	31.5	w
ν_{as} CH_2 (E)	2974.2	22.8	22.9	w	2974.3	22.9	12.5	w
ν_{as} CH_2 (A)	2983.9	27.1	26.8	w	2983.9	28.7	28.2	w
ν_{as} CH_3 (E)	3003.3	21.5	21.8	w	2993.6	36.5	39.1	w
ν_{as} CH_3 (A)	3013.0	31.9	30.5	w	3022.7	25.2	21.3	w
ν_{as} CH_3 (C)	3051.7	25.1	27.9	w	3051.7	72.2	69.7	w
ν_s CH (E)	3061.4	50.5	50.1	w	3061.4	53.5	55.4	w
ν_s CH (A)	3071.1	49.6	50.8	w	3071.1	50.8	26.8	w
ν_s CH (C)	3080.8	20.3	21.0	w	3080.8	52.8	55.9	w
ν_s CH (D)	3090.5	39.8	41.0	w	3090.5	41.0	20.4	w
ν_s CH (B)	3100.2	15.6	15.6	w	3109.9	13.0	10.1	w
ν_{as} CH (A,B,C,D,E)	$3110 \div 3200$	5.3	5.2	w	$3110 \div 3200$	3.8	3.8	w

assumed by this mesogen in its N_u and N_b phases. All this considered, it is also important to note that although the shape may change from BS to HSS (or vice versa) as a function of temperature, this does not necessarily mean that the phase type has changed. Also a change in the conformer populations could occur even far from the $N_u - N_b$ phase transition.

C. Magnetic Susceptibility Tensor Calculations

One of the most interesting aspects in bent-core LC, in fact, is to understand how these molecules are organized and packed in the bulk phase and in the presence of an external magnetic field. Knowledge of the anisotropy part $\Delta\chi^{Mol}$ of the molecular magnetic susceptibility χ^{Mol} of the molecule is necessary for the determination of how the mesophase director(s), especially in the case of a N_b phase, aligns in an external magnetic field. Usually, the magnetic field is not strong enough to orient a single molecule or isolated molecules: the interaction energy, due to cooperative molecular ordering, is indeed crucial [35]. Moreover, in bulk LC the molecular magnetic susceptibility is much different from the phase magnetic susceptibility, which is a quantity averaged over all motions of molecules in the LC phase. However, the symmetry properties of the molecular magnetic susceptibility tensor can help in understanding the differences, at a molecular level, when a N_u or a N_b phase is formed. At a macroscopic level, the magnetic energy density of the system can be expressed as $g_M = -\chi_a(\vec{H}\cdot\vec{n})^2/(2\mu_0)$, where μ_0 is the universal permittivity in vacuum, and χ_a is the anisotropy of the magnetic susceptibility, defined as $\chi_a = \chi_{\parallel} - \chi_{\perp}$, with $\chi_{\parallel}$ and $\chi_{\perp}$ denoting the components of the phase magnetic susceptibility tensor parallel and perpendicular to the director, respectively. The direction of preferred alignment of a system in the magnetic field depends on the sign of the anisotropy χ_a. Positive χ_a values seen in most liquid crystals result in the alignment of the phase director $\vec{n}$ parallel to the magnetic field $\vec{H}$; on the contrary, negative sign of χ_a can often be easily seen in discotic and calamitic liquid crystals constituted only of aliphatic parts. In principle it is possible to relate the macroscopic property χ_a to the molecular property $\Delta\chi^{Mol}$ as well as the Saupe order parameters S [36]. The case of V-shaped molecules is less obvious, since the molecular shape of these molecules is in a way intermediate between the previous cases [37]. This makes it difficult to properly choose the direction of the long molecular axis, which could be one of the reasons why these molecules could form biaxial phases.

In this section, we show that the molecular magnetic susceptibility anisotropy $\Delta\chi^{Mol}$ is strictly dependent on the molecular conformation. The implication of the average molecular conformation is strongly related to the orientation of banana molecules in a magnetic field, as also found for other bent-core mesogens with molecular structures more symmetric than that of A131. In particular, the two main conformational states found for A131, BS ($\boldsymbol{\Gamma_1}$, $\boldsymbol{\Gamma_4}$) and HSS ($\boldsymbol{\Gamma_2}$, $\boldsymbol{\Gamma_3}$), give two distinct magnetic susceptibility tensors, whose asymmetric terms are $\eta_{\chi^{MOL}} \sim 0.15$ and $\eta_{\chi^{MOL}} \sim 0.55$, respectively (see Table 4). These results are put in evidence in Figure 5, where the PASs of the MSTs in each conformation are shown. Here the axes of each PAS represent the eigenvectors of the the MST of each conformer, with magnitude value given in a coloured scale. Of course, uniaxial and biaxial MSTs can be easily distinguished by the number of different coloured axes that they posses: two different axes in the case of uniaxial $\boldsymbol{\Gamma_1}$ and $\boldsymbol{\Gamma_4}$ conformations, while three in the case of $\boldsymbol{\Gamma_2}$ and $\boldsymbol{\Gamma_3}$ ones.

Table 4. Molecular magnetic susceptibility tensor parameters [cgs-ppm] for the systems: 5CB, 5OCB (used for comparison) and for the investigated $\boldsymbol{\Gamma_i}$ (with i = 1,2,3,4) conformers and for the complete A131 molecule with the aromatic core in its four main different conformational states: $\boldsymbol{\Gamma_1}$, $\boldsymbol{\Gamma_2}$, $\boldsymbol{\Gamma_3}$ and $\boldsymbol{\Gamma_4}$. χ_{ii} are the principal components, χ^{iso} is the isotropic value, $\Delta\chi = \chi_{YY} - 1/2(\chi_{XX} + \chi_{ZZ})$ is the anisotropy part and $\eta_\chi = \frac{\chi^o_{11} - \chi^o_{22}}{\chi^o_{33}}$ is the asymmetry term). Note that χ^o_{11}, χ^o_{22} and χ^o_{33} are the principal components of the traceless MST, ordered according to the convention $|\chi_{33} - \chi^{iso}| \geq |\chi_{22} - \chi^{iso}| \geq |\chi_{11} - \chi^{iso}|$

System	χ_{XX}^{MOL}	χ_{YY}^{MOL}	χ_{ZZ}^{MOL}	χ^{iso}	$\Delta\chi^{MOL}$	η_χ^{MOL}
5CB	−141.6	−139.2	−224.8	−168.5	40.4	0.04
5OCB	−154.3	−144.9	−228.6	−175.9	32.5	0.23
$\boldsymbol{\Gamma_1}$	−327.4	−168.6	−346.8	−280.9	168.5	0.17
$\boldsymbol{\Gamma_2}$	−254.3	−185.7	−405.8	−281.9	144.4	0.54
$\boldsymbol{\Gamma_3}$	−256.9	−188.7	−397.4	−280.9	138.5	0.59
$\boldsymbol{\Gamma_4}$	−326.7	−167.8	−345.0	−279.8	168.0	0.15
A131($\boldsymbol{\Gamma_1}$)	−509.4	−350.6	−528.8	−462.9	168.5	0.16
A131($\boldsymbol{\Gamma_2}$)	−438.3	−367.7	−589.8	−465.3	146.4	0.56
A131($\boldsymbol{\Gamma_3}$)	−437.9	−373.7	−582.4	−464.7	136.5	0.54
A131($\boldsymbol{\Gamma_4}$)	−511.7	−349.8	−527.0	−462.9	169.5	0.12

In Table 4, molecular magnetic susceptibility tensors of the uniaxial $\boldsymbol{\Gamma_1}$, $\boldsymbol{\Gamma_4}$ (**5R** model) conformers and the whole A131 molecule in these conformations, A131($\boldsymbol{\Gamma_1}$), A131($\boldsymbol{\Gamma_4}$) are seen to be clearly distinguishable from those of the biaxial conformers

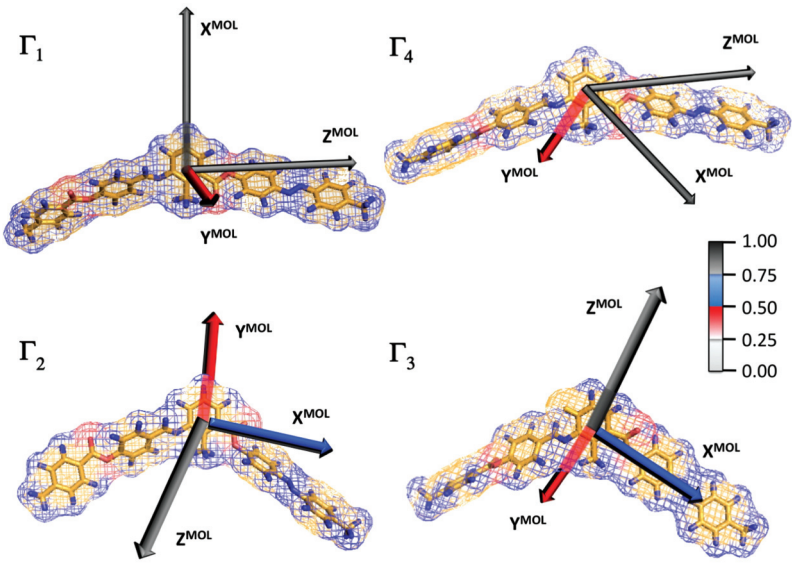

Figure 5. Molecular Magnetic Susceptibility Tensors (MSTs) defined in their PAS for each main populated conformational state in A131. Here the axes of each PAS represent the eigenvectors of the the MST of each conformer, with normalized intensity value given in a coloured scale (scale 1.00 means most negative value for the MST eigenvalue).

$\boldsymbol{\Gamma_2}$, $\boldsymbol{\Gamma_3}$ and the whole molecule of A131 in these conformations, A131($\boldsymbol{\Gamma_2}$) and A131($\boldsymbol{\Gamma_3}$). It is important to notice that the MSTs calculated for the full molecule of A131 in the $\boldsymbol{\Gamma_i}$ conformation where an isotropic shift-factor of ~180 cgs-ppm has to be applied for the presence of the aliphatic chains, are approximately the same as those obtained for the corresponding conformation in the **5R** model (in general the aliphatic portions of the molecule do not alter the anisotropy but only the isotropic part of the MST). Generally, both the isotropic and the anisotropic parts of the MST obtained for A131 conformers are comparable with those calculated for another series of banana molecules with similar molecular structures [38]. Moreover, note that $\Delta\chi^{Mol}$ of the A131 molecule is larger by a factor of ca. 4 when comparing with those of conventional uniaxial rod-like mesogens like 5CB and 5OCB listed in the same table. In summary, these preliminary results reveal that molecular magnetic susceptibilities in A131 are conformationally dependent, which may lead to potential interest for explaining differences between the N_u and N_b phases. They may also be used to calculate the phase magnetic susceptibility, once suitable models are available for the structures of N_u and N_b phases exhibited by A131. Future work will be pursued in this direction by exploiting molecular field theory.

D. Chemical Shielding Tensor Calculations

Recent developments in ab initio methods and computer hardware have made accurate evaluation of NMR chemical shieldings of many molecular systems possible. In particular, the quantum mechanical methodologies have now matured to such an extent that the results of ab initio calculations can significantly enhance the information obtainable from NMR spectra, increasing its interpretative power especially in the case of ^{13}C NMR of different type of liquid crystalline systems [39–42].

The CSA tensors calculated using fully relaxed structures of the **5R** model from the in vacuo DFT method for $\boldsymbol{\Gamma_1}$ and $\boldsymbol{\Gamma_3}$ (for the sake of brevity) of the four relevant ($\boldsymbol{\Gamma_1}$, $\boldsymbol{\Gamma_2}$, $\boldsymbol{\Gamma_3}$ and $\boldsymbol{\Gamma_4}$) conformers are compared in Table 5 with experimental principal components of the CSA tensors for some carbon sites in A131 [15]. The accuracy of each CSA component evaluated from 2D SUPER powder patterns of A131 is ca. ±3 ppm. The Root Mean Squared Deviation (RMSD) evaluated among the $\boldsymbol{\Gamma_i}$ conformers is ca. ±1 ppm for all the conformations, showing that there are no significant dependences of the CSA tensors on the different conformational states. As seen in the table, the differences are mainly observed for the carbons (C11, C12, C13, C14, C15, C17 and C26) located at the central ring **C** and close to it. When the ϕ_4 and ϕ_5 dihedrals are scanned among the different conformers, the local electron densities of the chemical bonds involved in the rotations, have indirectly influenced the local electron density of the central ring **C** to produce the above observation. It is noticed that the PAS's orientations of all the CST in different conformations are close to those expected from the standard geometry (e.g., the β angle for a protonated carbon on a phenyl ring is 60°) to within two degrees [30].

When comparing the experimental CSA with the DFT tensors, the Root Mean Squared Error (RMSE) are about 3, 6, 5 and 4 ppm for δ_{iso}, δ_{11}, δ_{22} and δ_{33}, respectively, if we exclude those of carbons C3, C7, C11, C22 and C23, which show fairly noisy SUPER powder patterns [15]. If the comparison is extended to all the aromatic carbons of A131, the evaluated RMSEs for δ_{iso}, δ_{11}, δ_{22} and δ_{33} are 3, 10, 14 and 13, respectively, indicating that the experimental CSAs for carbons C3, C7, C11, C22

Table 5. Experimental (revised from Ref. [15]), and calculated (GIAO-DFT) chemical shift tensors for Γ_i conformers of aromatic carbon sites of A131

		δ^{Iso}	δ_{33}	δ_{22}	δ_{11}			δ^{Iso}	δ_{33}	δ_{22}	δ_{11}			δ^{Iso}	δ_{33}	δ_{22}	δ_{11}			δ^{Iso}	δ_{33}	δ_{22}	δ_{11}			δ^{Iso}	δ_{33}	δ_{22}	δ_{11}
	exp	149.4	–	–	–		exp	122.4	211.1	145.9	11.7		exp	123.6	203.5	145.0	25.1		exp.	152.3	244.6	149.0	71.0		exp.	123.6	203.5	145.0	25.1
C1	Γ_1	145.7	249.4	180.7	7.0	**C6**	Γ_1	120.5	211	136.9	13.6	**C11**	Γ_1	121.9	216.1	131.9	17.7	**C17**	Γ_1	155.1	251.7	140.8	72.7	**C22**	Γ_1	124.1	219.0	146.3	7.1
	Γ_3	145.8	249.5	181.0	7.0		Γ_3	121.3	210.5	139.8	13.6		Γ_3	121.3	214.8	131.3	17.7		Γ_3	154.1	251.4	138.1	72.7		Γ_3	124.2	218.8	146.7	7.1
	exp	129.1	224.9	137.9	28.5		exp	130.5	213.6	170.9	17.2		exp	126.5	–	–	–		exp	122.4	211.1	145.9	11.7		exp	130.5	191.4	159.9	47.4
C2	Γ_1	128.5	232.7	135.6	17.3	**C7**	Γ_1	131.1	233.8	150.7	8.8	**C12**	Γ_1	125	232.9	136.0	6.2	**C18**	Γ_1	121.3	211.4	138.4	14.0	**C23**	Γ_1	129.2	232.6	133.9	21.0
	Γ_3	128.3	232.4	135.1	17.3		Γ_3	130.8	233.0	150.5	8.8		Γ_3	125.4	232.8	137.3	6.2		Γ_3	121.1	211.4	137.9	14.0		Γ_3	129.4	233.0	134.1	21.0
	exp	130.5	213.6	170.9	17.2		exp	129.1	219.3	147.4	14.6		exp	129.1	224.9	137.9	28.5		exp	124.5	210.2	168.2	−2.7		exp	146.3	–	–	–
C3	Γ_1	132.7	237.6	154.2	6.2	**C8**†	Γ_1	132.4	219.0	167.7	10.4	**C13**	Γ_1	131.2	235.4	148.9	9.1	**C19**	Γ_1	124.5	218.2	148.2	7.0	**C24**	Γ_1	142.8	247.6	172.3	8.3
	Γ_3	132.2	237.0	153.4	6.2		Γ_3	132.8	219.9	168.1	10.4		Γ_3	130.8	239.3	143.9	9.1		Γ_3	124.4	217.7	148.7	7.0		Γ_3	142.8	247.7	172.4	8.3
	exp	126.5	217.8	135.3	30.4		exp	159.0	245	163	70		exp	134.5	214.6	160.6	30.2		exp	151.2	236.4	158.4	57.9		exp	164.9	267.8	117.1	106.6
C4	Γ_1	126.3	216.4	140.6	22.0	**C9**%	Γ_1	158.7	237.5	161.8	76.7	**C14**	Γ_1	128.7	216.6	140.3	29.1	**C20**	Γ_1	150.2	232.1	174.7	43.8	**C25**	Γ_1	163.7	263.3	123.5	104.2
	Γ_3	126.3	216.2	140.7	22.0		Γ_3	158.9	238.2	161.9	76.7		Γ_3	130.4	218.4	143.6	29.1		Γ_3	151.0	232.8	176.3	43.8		Γ_3	163.5	264.8	121.5	104.2
	exp	154.1	243.5	150.5	66.5		exp	152.3	241	173	35.5		exp	134.5	–	–	–		exp	151.2	239.4	164.5	43.0		exp	164.9	270.0	112.6	102.1
C5	Γ_1	153.9	249.4	141.5	70.7	**C10**#	Γ_1	153.3	235.7	178.6	45.4	**C15**	Γ_1	142.4	222.2	190.0	15.0	**C21**	Γ_1	151.1	234.1	176.9	42.4	**C26**	Γ_1	164.0	265.5	117.1	109.3
	Γ_3	154.0	249.7	141.6	70.7		Γ_3	152.9	235.6	177.8	45.4		Γ_3	137.7	214.2	184.0	15.0		Γ_3	151.6	234.2	178.2	42.4		Γ_3	167.3	270.7	121.8	109.3

% Reference [43], †Reference [44], #Reference [45].

and C23 must be taken with some caution. Moreover, the relative values of CSA components found for these carbons have the largest deviations from those commonly found in carbons having the same topology and chemical nature [43]. Note that experimental CSAs were determined in the solid phase, while the DFT calculations were performed in vacuo, which did not account for the effect of molecular packing in the mesophase. Though carbon-13 is likely not to be affected by the packing effects, this could, however, represent a source of deviation between the calculated (DFT) and experimental CSA tensors [42]. One conclusion from these chemical shielding calculations when compared with the experimental CSAs is that the conformers found from the PES are indirectly shown as reasonable representations of the A131 molecular core.

E. Orientational Order Parameters

The ^{13}C $\langle\delta\rangle$ in mesophases is related to its isotropic δ_{iso} value by Eq. (2) for all aromatic carbon sites except for the central ring, where Eq. (3) is used instead. To fit the observed $\langle\delta\rangle$'s in the nematic phases, the CSA values listed for A131 in Table 5 can be used. For the central ring, S_{xz} is found to be vanishingly small (ca. 0.1) for all the studied temperatures. When the derived Saupe matrix for the central ring is diagonalized to give its S and D, the principal axes of its PAS can also be located. The orientation of the original z axis is found to only shift by less than two degrees on average towards the C12-C26 bond. This small change in the z direction is a result of the small S_{xz} value.

Now all possible sets of CSA tensors were tested. We found that the fits to the chemical shifts $<\delta>$'s are quite similar for all the cases in which DFT CSA tensors of a particular conformer were used. No substantial difference were found when calculating order parameters using "regular" or DFT calculated geometry for the orientations of the shielding tensors, as found in ZLL 7/* mesogen [41]. For this reason, we have adopted below the "regular" geometry. Thus the set of CSA tensors for the $\boldsymbol{\Gamma_3}$ conformer (note those of $\boldsymbol{\Gamma_4}$ are just as good) is chosen here as an example in fitting the chemical shift data. Fitting 21 carbon sites (C1-C8, C10-C15, and C17-C24) using only the $\boldsymbol{\Gamma_3}$ DFT tensors, the goodness of fits to all 13 chosen temperatures in the mesophases is measured by the Sum Squared Deviation (SSD). The SSD evaluated in this case was 1258 (this corresponds to a RMSD value of about 2.2 ppm on the average for each carbon(s) at each temperature). As DFT tensors were derived in-vacuo, we next tried to use all the experimentally available CSA tensors in fitting the same data set, but noting that when experimental CSA is unavailable for C1, C12, C15 and C24, the corresponding CSA of $\boldsymbol{\Gamma_3}$ was used, while the CSA for C8 was from Ref. [44]. The fits were indeed improved somewhat to give a lower SSD of 1136 (which corresponds to a RMSD value of ca. 2.0 ppm). To understand this, it would appear that the in vacuo CSA tensors may not be reflecting the slight perturbation due to the existence of packing or medium effects, even if this effect should be considered very small as found in Ref. [41]. On the other hand, as pointed out above some of the CSA tensors derived from noisy powder patterns (due to spectral overlaps and limited sample volume) may not be too reliable. To check this possibility, we then replaced those of C7, C19, C22 and C23 by their corresponding $\boldsymbol{\Gamma_3}$ CSA values (this corresponds to the best outcoming) for fitting the same set of ^{13}C $\langle\delta\rangle$'s. Indeed, the SSD of the new fits yields the best value of 1016 (which

corresponds to a RMSD of 1.9 ppm) [16,30]. Though DFT CSA tensors are more or less indpendent of the chosen Γ_i, it should be pointed out in vacuo Γ_1 has lower potential energy and higher population, and is supposed to be likely closer to the average shape of an A131 molecule in the uniaxial N_u phase. Though the more bent Γ_3 (Γ_2) structure is less populated in vacuo, it could become increasingly populated due to molecular packing in the condensed phase at low temperatures as suggested below. The hockey-stick shape, ($\Theta = 116°$) can likely become a dominant conformer, at least in view of the existing theory, in the N_b phase.

It has been shown [30] that different choices of CSA values do influence the derived local order parameters S and D somewhat. Here, the best set of calculated local order parameters (see Fig. 6(a)) as a function of the temperure are used to discuss the conformation state of the A131 molecular core. Notice that S (only ring **B** and **D** are given) increases with decreasing temperature for all rings in the N_u phase and tends to level off in the N_b phase, while D's are negative in the N_b phase for all rings except ring **D**. The local S of ring **D** remains the largest among all aromatic rings as noted previously [15] for almost the entire temperature range. Thus its para axis is closest to the 'long' molecular axis. There exist discontinuous jumps in S at 422 K as seen in Figure 6(a) for ring **B** and **D**.

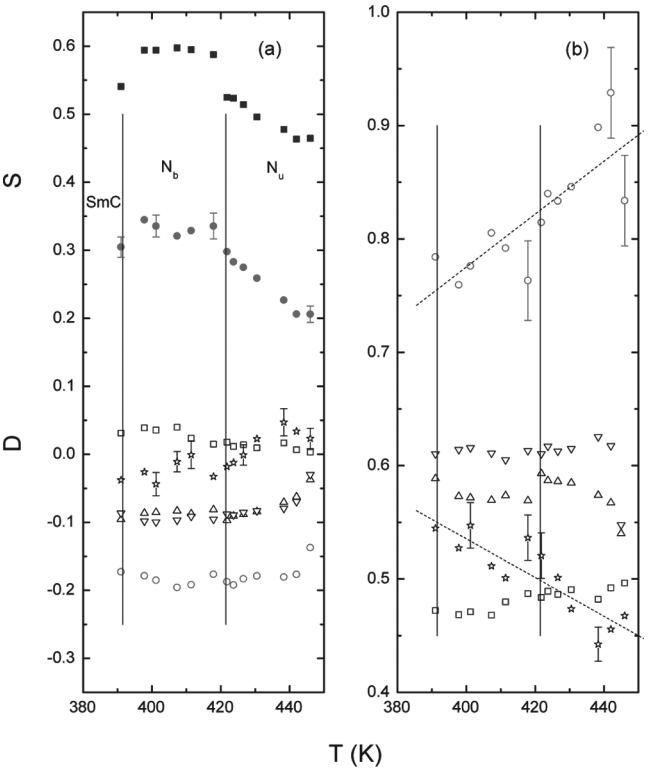

Figure 6. (a) Plots of local order parameters S (only for rings **B** (●) and **D** (■) for clarity) and biaxial order parameters D of rings **A** (*), **B** (○), **C** (Δ), **D** (□), and **E** (▽) using SUPER CSA tensors and 8 CSA tensors calculated for Γ_3 conformer (see text). (b) Plots of 'normalized' local order parameters $\rho = -S_{xx}/S$ of rings **A** (*), **B** (○), **C** (Δ), **D** (□), and **E** (▽). Lines are drawn to aid the eyes and some typical error bars are given.

It is interesting to examine the behaviors of local biaxial order parameters D in the low temperature N phase, particularly for ring **D**. This is because the D parameter reflects the relative degree of ordering of the two minor fragment axes x and y with respect to the major director. Note that ring **B** has the largest absolute D value, i.e., largest local biaxiality (or S_{yy} tends to zero), that is relatively insensitive to the temperature, and a smallest S value among all the rings. This observation can be explained by taking into account two distinct observations: (i) the energy barriers for rotation of ring **B** around the dihedral angles ϕ_2 and ϕ_3 are very low (ca. 2 kcal/mol), [30] as found in the DFT calculations, and (ii) the orientation of para axis of ring **B** is highly tilted (it forms an angle of about 60°, because the rotation of ring **B** around ϕ_4 is restricted, due to the presence of the methyl (C_{16}) unit in ring **C**). It is interesting to note that only ring **D** has positive D values (ca. 0.03) in the N_b phase. Furthermore, D of ring **A** appears to go through zero at the $N_u - N_b$ phase transition and becomes slightly positive in the N_u phase. Physically, this implies the ring **D**'s normal (y axis) to its ring plane is twisted in the opposite sense with respect to those of other rings in the N_b phase (same can be said about ring **A** in the N_u phase). Perhaps these two rings (**A** and **D**) are involved in providing symmetry breaking at the uniaxial to biaxial phase transformation.

To further shed light on the local orientational behaviors of various rings in A131 bent-core, we have plotted $-S_{xx}/S$, a normalized local order (ρ) of the x axis, as a function of temperature in Figure 6(b). Note that ρ has two extreme limits: (i) when S_{yy} tends to zero, ρ has a limiting value of one corresponding to maximal ordering of the x axis relative to the major director, (ii) when $D = 0$, then $S_{xx} = S_{yy} = -S/2$ and ρ approaches a limiting value of 0.5. Now ρ of rings **C, D** and **E** are relatively insensitive to temperature over the nematic range (slightly less so for ring **D**), while **A** and **B** rings show substantial, and opposite temperature behaviors. Though the reported $N_u - N_b$ transition at around 422 K may not be discerned in this plot, it is clear that these two rings (perhaps also ring **D**) are responsible for changing the populations of two (or more) dominant conformers with the

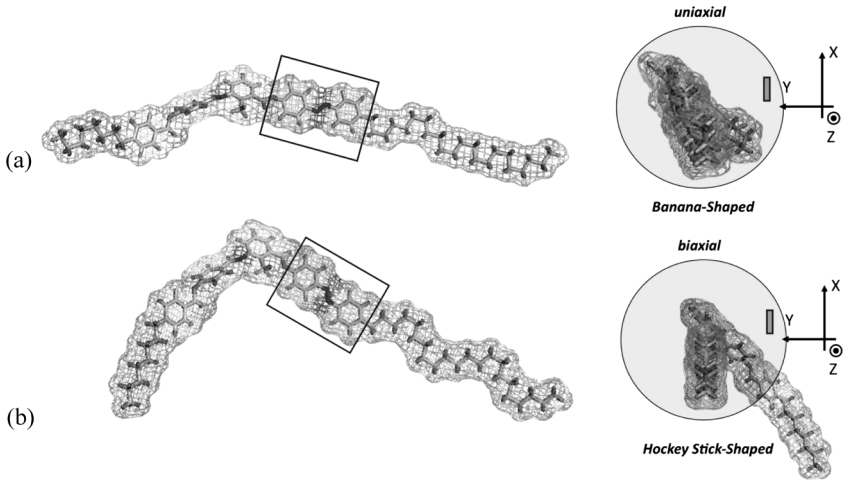

Figure 7. Schematics of A131 molecule in (a) its uniaxial 'banana-shaped' conformation and in (b) its biaxial 'hockey stick'-shaped conformation. The cage indicates the surface accessible to the solvent.

temperature. Besides the equilibrium populations of two (or more) distinct configurations for A131 core can vary, it would seem that the flexible end chains must also play a role in shaping the overall configuration of the V-shaped molecule. The chains should mediate the molecular packing in the underlying SmC phase and also likely in the N_b phase.

IV. Conclusion

The $N_u - N_b$ phase transition in the bent-core A131 mesogen has recently been casted in doubt by an electro-optic study. It was suggested that the observed transition in the X rays work is related to surface anchoring transition. A careful analysis of the ^{13}C chemical shifts $\langle\delta\rangle$'s has demonstrated that the normalized local order parameter ρ of ring **A** and **B** have shown quite strong and opposite temperature behaviours. The existence of more than one conformer is clear both from the in vacuo DFT calculations and local order parameters obtained by ss-NMR. Four prevalent conformations (and four symmetry related ones) showing two different bent-core shapes have been revealed. Note that the conformational average of the molecular shape must depend on the Boltzmann distribution. Our current NMR study seems to support a phase transition at 422 K, but has no way to decide on a biaxial nematic phase below this transition, as only molcular biaxial order D can be deduced. The non-zero phase biaxial order parameters if exist, are not accessible in the present study.

Now a group of conformers has a bend angle close to 143° and a configuration more like a "banana"-shaped conformer. The other group has a smaller bend angle of about 116° and resembles more like a hockey stick-shaped structure. When adding the flexible chains to the A131 bent-core as shown in Figure 7 and viewing along its "long" axis, the former appears like a uniaxial rod, while the latter more like a biaxial object. The schematized molecular shapes are inferred from subtle changes in the orientations of rings **A, B**, and **D** that occur in these two nematic phases. In conclusion, the present study points to the mix of two (or more) different conformers being a potential souce for a uniaxial-biaxial nematic transition as suggested by a recent theory. Moreover, the two different molecular magnetic susceptibility tensors obtained for the BS and the HSS conformations could be potentially used for calculating the phase magnetic susceptibility, once suitable models for the N_u and N_b structures in A131 become available. Finally, we suggest that a possible way to distinguish the BS and HSS in A131 is to record its IR spectra in the two nematic phases, even though it's worth noting that although the shape may change from BS to HSS (or vice versa) as a function of temperature, this does not necessarily mean that the phase type has changed.

Acknowledgments

R.Y.D. thanks the Natural Sciences and Engineering Council of Canada for financial support, and A.M. is particularly grateful to Prof. C. A. Veracini and Prof. B. Mennucci for useful discussion.

References

[1] Freiser, M. J. (1970). *Phys. Rev. Lett.*, *24*, 1041.
[2] Yu, L. J. & Saupe, A. (1980). *Phys. Rev. Lett.*, *45*, 1000.

[3] Luckhurst, G. R. (2001). *Thin Solid Films*, *393*, 40.
[4] Madsen, L. A., Dingemans, T. J., Nakata, M., & Samulski, E. T. (2004). *Phys. Rev. Lett.*, *92*, 145505.
[5] Acharya, B. R., Primak, A., & Kumar, S. (2004). *Phys. Rev. Lett.*, *92*, 145506.
[6] Lee, J.-H., Lim, T.-K., Kim, W.-T., & Jin, J.-I. (2007). *J. Appl. Phys.*, *101*, 034105.
[7] Niori, T., Sekine, F., Watanabe, J., Furukawa, T., & Takezoe, H. (1996). *J. Mater. Chem.*, *6*, 1231.
[8] Pelzl, G., Diele, S., & Weissflog, W. (1999). *Adv. Mater. (Weinheim, Ger.)*, *91*, 707.
[9] Dingemans, T. J., & Samulski, E. T. (2000). *Liq. Cryst.*, *27*, 131.
[10] Fodor-Csorba, K., Vajda, A., Jakli, A., Slugovc, C., Trimmel, G., Demus, D., Gacs-Baitz, E., Holly, S., & Galli, G. (2004). *J. Mater. Chem.*, *14*, 2499.
[11] Teixeira, P. I. C., Masters, A. J., & Mulder, B. M. (1998). *Mol. Cryst. Liq. Cryst.*, *323*, 167.
[12] Bates, M. A., & Luckhurst, G. R. (2005). *Phys. Rev. E*, *72*, 051702.
[13] Bates, M. A. (2006). *Phys. Rev. E*, *74*, 061702.
[14] Prasad, V., Kang, S.-W., Suresh, K. A., Joshi, L., Wang, Q., & Kumar, S. (2005). *J. Am. Chem. Soc.*, *127*, 17224.
[15] Dong, R. Y., Kumar, S., Prasad, V., & Zhang, J. (2007). *Chem. Phys. Lett.*, *448*, 54. This preliminary report unfortunately has missed a scaling factor of 0.667 for the isotropic chemical shifts.
[16] Dong, R. Y., & Marini, A. (2009). *J. Phys. Chem. B*, *113*, 14062.
[17] Van Le, K., Mathews, M., Chambers, M., Harden, J., Li, Q., Takezoe, H., & Jakli, A. (2009). *Phys. Rev. E*, *74*, 030701(R).
[18] Keith, T. A., & Bader, R. F. W. (1993). *Chem. Phys. Lett.*, *210*, 223.
[19] Cheeseman, J. R., Trucks, G. W., Keith, T. A., & Frisch, M. J. (1996). *J. Chem. Phys.*, *104*, 5497.
[20] Gaussian 03, Revision B.05, M. J. Frisch et al., Gaussian, Inc., Pittsburgh PA, 2003.
[21] Ditchfield, R. (1972). *J. Chem. Phys.*, *56*, 5688.
[22] Dong, R. Y., Xu, J., Zhang, J., & Veracini, C. A. (2005). *Phys. Rev. E*, *72*, 061701.
[23] (a) Becke, A. D. (1988). *Phys. Rev. A*, *38*, 3098; (b) Lee, C., Yang, W., & Parr, R. G. (1988). *Phys. Rev. B*, *37*, 785; (c) Stephens, P. J., Devlin, F. J., Chabalowski, C. H., & Frisch, M. (1994). *J. Phys. Chem.*, *98*, 11623.
[24] Wrzalik, R., Merkel, K., & Kocot, A. (2003). *J. Mol. Model*, *9*, 248.
[25] Wiberg, K. B. (1999). *J. Comput. Chem.*, *20*, 1299.
[26] Perdew, J. P. (1991). In: *Electronic Structure of Solids*, Ziesche, P. & Eschig, H. (Eds.), Akademie Verlag: Berlin, 11.
[27] (a) Adamo, C., & Barone, V. (1998). *J. Chem. Phys.*, *108*, 664; (b) Lynch, B. J., Zhao, Y., & Truhlar, D. G. (2003). *J. Phys. Chem.*, *107*, 1384.
[28] Gauss, J. (1993). *J. Chem. Phys.*, *99*, 3629.
[29] Mason, J. (1987). *Multinuclear NMR*, Plenum Press: New York, Chap. 3.
[30] Marini, A., Prasad, V., & Dong, R. Y. (2009). A combined DFT and carbon-13 NMR study of a biaxial bent-core liquid crystal. In: *Nuclear Magnetic Resonance Spectroscopy of Liquid Crystals*, Dong, Ronald Y. (Ed.), World Scientific Publishing Co.: Singapore.
[31] Dewar, M. J. S., Jie, C. X., & Yu, J. G. (1993). *Tetrahedron*, *49*, 5003.
[32] Cramer, C. J. (2004). *Essentials of Computational Chemistry*, 2nd Ed., J. Wiley & Sons, Ltd.
[33] Merrick, J. P., Moran, D., & Radom, L. (2007). *J. Phys. Chem. A*, *111*, 11683.
[34] Merkel, K., Kocot, A., Vij, J. K., Mehl, G. H., & Meyer, T. (2004). *J. Chem. Phys.*, *121*, 5012.
[35] de Gennes, P. G., & Prost, J. (1993). In: *The Physics of Liquid Crystals*, Clarendon: New York, 57–58.
[36] Saupe, A., & Englert, G. (1966). *Mol. Cryst. Liq. Cryst.*, *1*, 503.
[37] Domenici, V., Veracini, C. A., & Zalar, Bostjan (2005). *Soft Matter*, *1*, 408.

[38] Domenici, V., Veracini, C. A., Fodor-Csorba, K., Prampolini, G., Cacelli, I., Lebar, A., & Zalar, Bostjan (2007). *Chem. Phys. Chem.*, *8*, 2321.
[39] Catalano, D., Geppi, M., Marini, A., Veracini, C. A., Urban, S., Czub, J., Kuczynski, W., & Dabrowski, R. (2007). *J. Phys. Chem. C*, *111*, 5286.
[40] Geppi, M., Marini, A., Veracini, C. A., Urban, S., Czub, J., Kuczynski, W., & Dabrowski, R. (2008). *J. Phys. Chem. B*, *112*, 9663.
[41] Dong, R. Y., Geppi, M., Marini, A., Hamplova, V., Kaspar, M., Veracini, C. A., & Zhang, J. (2007). *J. Phys. Chem. B*, *111*, 9787.
[42] Marini, A. (2009). *Structure, Orientational Order and Magnetic Properties from Simple to Complex Liquid Crystalline Materials: A Combined Multinuclear NMR Spectroscopy and ab Initio Calculations Approach*, 26 June, Pisa (Italy).
[43] Duncan, T. M. (1997). *Principal Components of Chemical Shielding Tensors: A compilation*, 2nd Ed., The Farragut Press: Madison, WI.
[44] Zheng, G., Hu, J., Zhang, X., Shen, L., Ye, C., & Webb, G. A. (1998). *J. Mol. Struct.*, *428*, 283.
[45] Parhami, P., & Fung, B. M. (1985). *J. Am. Chem. Soc.*, *107*, 7304.